Bull. Mater. Sci., Vol. 36, No. 3, June 2013, pp. 395–401. © Indian Academy of Sciences.

Electrical conductivity and chemical stability of $BaCe_{0.8-x}A_xGd_{0.2}O_{3-\delta}$ (A = In, Zr, Ta; x = 0, 0·1) ceramics

XIAO-MING LIU, YI-JING GU, ZHAN-GUO LIU, JIA-HU OUYANG*, FU-YAO YAN and JUN XIANG

School of Materials Science and Engineering, Harbin Institute of Technology, 92 West Da-Zhi Street, Harbin 150001, P. R. China

MS received 3 August 2011; revised 4 February 2013

Abstract. **$BaCe_{0.8-x}A_xGd_{0.2}O_{3-\delta}$ (A = In, Zr, Ta; x = 0, 0·1) ceramics were synthesized by solid-state reaction method. Microstructure and electrical properties of $BaCe_{0.8-x}A_xGd_{0.2}O_{3-\delta}$ ceramics were investigated by means of X-ray diffraction (XRD), scanning electron microscopy (SEM) and complex impedance analysis at intermediate temperatures of 573–1073 K in different atmospheres. $BaCe_{0.8}Gd_{0.2}O_{3-\delta}$, $BaCe_{0.7}In_{0.1}Gd_{0.2}O_{3-\delta}$ and $BaCe_{0.7}Zr_{0.1}Gd_{0.2}O_{3-\delta}$ ceramics exhibit a single cubic perovskite structure. $BaCe_{0.7}In_{0.1}Gd_{0.2}O_{3-\delta}$ ceramic has the highest conductivity of $4{\cdot}6 \times 10^{-2}$ S·cm^{-1} in air at 1073 K. $BaCe_{0.7}In_{0.1}Gd_{0.2}O_{3-\delta}$ and $BaCe_{0.7}Zr_{0.1}Gd_{0.2}O_{3-\delta}$ ceramics exhibit an excellent chemical stability against boiling water. Indium is a suitable doping element to promote the sintering densification and to enhance both electrical conductivity and chemical stability of Gd-doped $BaCeO_3$ at operating temperatures.**

Keywords. **Perovskite; solid electrolyte; impedance spectroscopy; electrical conductivity.**

1. Introduction

In recent years, fuel cells, in particular solid oxide fuel cells (SOFC), have received considerable attention due to their high efficiency and low environmental impact (Liou and Yang 2008; Zhang *et al* 2008; Khandelwal *et al* 2011). As an alternative electrochemical energy conversion devices, fuel cells convert chemical energy directly into electrical energy and their thermodynamic efficiencies are not restricted by the Carnot cycle (Kreuer 2003). Conventional SOFCs solid electrolytes are composed of ionic solid conductors, mostly 8 mol% yttria-stabilized zirconia (YSZ), which has a high oxide-ion conductivity and needs to operate approximately at 1273 K (Li *et al* 2010). Such a high operating temperature hinders their long-term stability and durability. Therefore, reducing the operation temperature of SOFCs is of great significance for the widespread use of fuel cells technology (Ishihara *et al* 2006; Liu *et al* 2010).

Proton conducting perovskite-type oxides have been considered as a promising alternative in view of decreasing operating temperature to the range of 773–973 K since the first observation of protonic conduction in some perovskite oxides by Iwahara (Iwahara *et al* 1981; Zuo *et al* 2006; Choudhury *et al* 2009; Jacob *et al* 2010). These perovskite oxides have great advantages over oxide–ion conducting compounds, such as low activation energy and high energy efficiency (Demin *et al* 2002). The activation energy for proton transport is about 0·3–0·6 eV, which is much smaller than that of 0·8 eV for the oxide–ion transport (Fabbri *et al* 2008). Furthermore, as water vapour is produced at the cathode side, no circulation of fuel gas is necessary for proton-conducting SOFCs. Among the proton conducting perovskite-type oxides, $BaCeO_3$ doped with rare-earth elements such as Gd, have been attracting increasing interest of many researchers due to its high proton conductivity in hydrogen- or water vapour-containing atmospheres at intermediate operation temperatures (Pelletier *et al* 2005; Chen and Ma 2009). Oxygen vacancies, which are directly responsible for oxide–ion conduction and protonic conduction are introduced into the perovskite structure when Ce^{4+} cations are substituted by the trivalent cations such as Y^{3+} and Gd^{3+}, the defect reaction in Krögern-Vink notation (Chiodelli *et al* 2009) is written as:

$$2Ce_{Ce}^{x} + Y_2O_3 + O_O^x \rightarrow 2Y'_{Ce} + V_O^{\bullet\bullet} + 2CeO_2. \quad (1)$$

The proton conduction in Gd-doped $BaCeO_3$ occurs due to dissociative adsorption of water or hydrogen in the presence of oxygen vacancies (Guan *et al* 1998; Kreuer 2003), according to the following equations:

$$H_2\,(g) + 2O_O^x \Leftrightarrow 2OH_O^{\bullet} + 2e', \quad (2)$$

$$H_2O\,(g) + V_O^{\bullet\bullet} + O_O^x \Leftrightarrow 2OH_O^{\bullet}. \quad (3)$$

A remarkable p-type electronic conductivity is also observed under oxidizing conditions (Zhang and Zhao 2010):

$$\frac{1}{2}O_2\,(g) + V_O^{\bullet\bullet} \Leftrightarrow O_O^x + 2h^{\bullet}. \quad (4)$$

*Author for correspondence (ouyangjh@hit.edu.cn)

These conductors exhibit a mixed ionic–electronic conductivity depending on temperature and environmental conditions (Norby and Larring 2000). It was reported that proton conductivity is predominant at low temperatures, while oxide-ion conductivity is the main contribution at high temperatures (Bonanos *et al* 1995). $BaCe_{1-x}A_xO_{3-\delta}$ ($A = Nd^{3+}$, Sm^{3+}, Gd^{3+}, Eu^{3+}, Yb^{3+}, Y^{3+} and In^{3+}) has been known to exhibit high conductivity (Virkar and Maiti 1985; Uehara *et al* 1987; Wu and Liu 1997; Chen *et al* 1998; Künstler *et al* 1998; Wang *et al* 2004; Peng *et al* 2006), however, good chemical stability is also required for practical applications as well as high conductivity. Unfortunately, doped $BaCeO_3$ have poor chemical stability at high operating temperatures in the presence of CO_2 and water vapour (Haile 2003; Mclntosh and Gorte 2004). To improve their chemical stability against CO_2 or H_2O, various doping strategies were tried. By suitable doping, these materials may obtain both high conductivity and sufficient chemical stability over a wide range of SOFC operating conditions. It was reported that partial substitution of In, Zr or Ta for Ce-site can improve the chemical stability of doped $BaCeO_3$. However, it remains unclear as to which is the most suitable doping element to improve both conductivity and chemical stability of Gd-doped $BaCeO_3$ under same conditions. In the present paper, $BaCe_{0.8-x}A_xGd_{0.2}O_{3-\delta}$ (A = In, Zr, Ta; $x = 0, 0{\cdot}1$) ceramics were synthesized by solid-state reaction method. The structure, electrical conductivity and chemical stability of $BaCe_{0.8-x}A_xGd_{0.2}O_{3-\delta}$ ceramics were then evaluated.

2. Experimental

$BaCe_{0.8-x}A_xGd_{0.2}O_{3-\delta}$ ($A = In, Zr, Ta$; $x = 0, 0{\cdot}1$) ceramics were synthesized by solid-state reaction method. High purity oxides of CeO_2, Gd_2O_3, In_2O_3, ZrO_2, Ta_2O_5 (Rare-Chem Hi-Tech Co. Ltd., China; purity $\geq$ 99·99%) and $BaCO_3$ (Tianjin Kermel Chemical Reagent Co. Ltd., China; purity $\geq$ 99%) powders were used as starting materials. A stoichiometric mixture of these raw materials was mixed and then ball milled with stabilized zirconia balls in analytically pure alcohol (Tianjin Kermel Chemical Reagent Co. Ltd., China; purity $\geq$ 99·5%) for 24 h. The weight ratio of ball to powder during ball milling is 2·5:1. After the solvents were evaporated, dried powders were subsequently calcined at 1523 K in air for 10 h. The calcined powder was then uniaxially pressed into pellets at 20 MPa, subsequently cold isostatically pressed at 200 MPa and then pressureless-sintered at 1973 K for 10 h in air.

The phase identification of the sintered pellets was performed by X-ray diffractometer (Rigaku D/Max 2200VPC, Japan) with Ni-filtered CuKα radiation. XRD patterns were recorded in 2θ range from 20–90° with a scan rate of 4°/min. The instrument was calibrated using pure silicon sample provided with instrument. Lattice parameters were obtained by refining XRD patterns with MDI Jade 5.0 software based on $BaCeO_3$ (PDF file no. 01-075-0431 International Centre for Diffraction Data). The fractured surfaces of $BaCe_{0.8-x}A_xGd_{0.2}O_{3-\delta}$ samples were observed using a field-emission scanning electron microscope (FEI Quanta 200F, the Netherlands) with an accelerating voltage of 30 kV. A thin carbon coating was evaporated onto the surfaces of the samples for SEM observations.

The electrical conductivity of $BaCe_{0.8-x}A_xGd_{0.2}O_{3-\delta}$ ceramics were investigated at intermediate temperatures of 573–1073 K in both air and dry hydrogen atmospheres by a.c. impedance spectroscopy using an impedance/gain-phase analyser (Solartron^{TM} SI 1260, UK) in the frequency range of 0·5 Hz–1 MHz with a perturbation amplitude of 10 mV. The data analysis was carried out by Zview 2 software with appropriate equivalent circuits. All the pellets for electrochemical measurements were polished into discs with dimensions of about 0·5 mm in thickness and 10 mm in diameter. Silver paste was placed on each side of the polished disc to form the electrode and then dried at 473 K for 15 min.

The chemical stability of $BaCe_{0.8-x}A_xGd_{0.2}O_{3-\delta}$ ceramics against water vapour was examined by comparing XRD patterns before and after exposing them in boiling water for 2 h. The sintered pellets were ground and polished into discs with dimensions of 2 mm in thickness and 10 mm in diameter.

3. Results and discussion

3.1 *Structural analysis of $BaCe_{0.8-x}A_xGd_{0.2}O_{3-\delta}$ ceramics*

XRD patterns of $BaCe_{0.8-x}A_xGd_{0.2}O_{3-\delta}$ ceramics sintered at 1973 K for 10 h are shown in figure 1. $BaCe_{0.8}Gd_{0.2}O_{3-\delta}$, $BaCe_{0.7}In_{0.1}Gd_{0.2}O_{3-\delta}$ and $BaCe_{0.7}Zr_{0.1}Gd_{0.2}O_{3-\delta}$ ceramics exhibit a single cubic perovskite structure (PDF 01-075-0431), while $BaCe_{0.7}Ta_{0.1}Gd_{0.2}O_{3-\delta}$ ceramic is composed of a cubic perovskite structure and a minor impurity phase of Gd_2O_3 (PDF 01-011-0608). The molar ratio of metallic elements in $BaCe_{0.8-x}A_xGd_{0.2}O_{3-\delta}$ ceramic measured by EDS and the lattice parameters extracted from

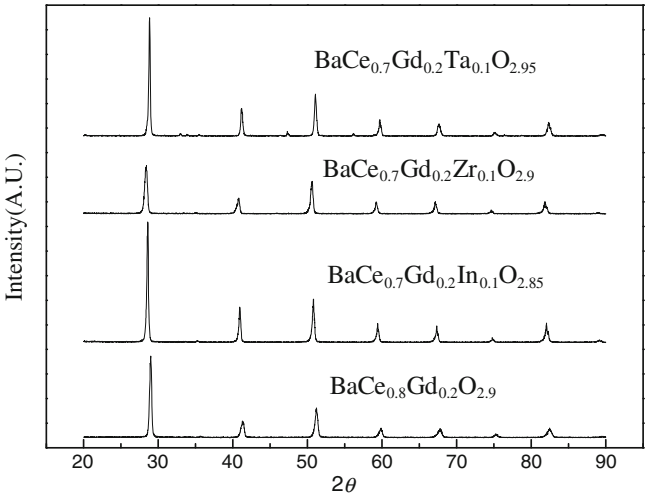

Figure 1. XRD patterns of $BaCe_{0.8-x}A_xGd_{0.2}O_{3-\delta}$ ceramics sintered at 1973 K for 10 h.

Table 1. Molar ratio of metallic elements and the lattice parameters in $BaCe_{0.8-x}A_xGd_{0.2}O_{3-\delta}$ ceramics sintered at 1973 K for 10 h.

Samples	Ba	Ce	Gd	In	Zr	Ta	a (Å)	V (Å^3)	Relative density (%)
$BaCe_{0.8}Gd_{0.2}O_{3-\delta}$	1·00±0·032	0·78±0·026	0·26±0·009	0	0	0	4·400±0·068	85·207±3·988	93±1·12
$BaCe_{0.7}In_{0.1}Gd_{0.2}O_{3-\delta}$	1·00±0·036	0·69±0·022	0·22±0·007	0·09±0·003	0	0	4·398±0·066	85·103±3·852	94±1·08
$BaCe_{0.7}Zr_{0.1}Gd_{0.2}O_{3-\delta}$	1·00±0·038	0·66±0·023	0·22±0·007	0	0·09±0·003	0	4·392±0·066	84·706±3·891	92±1·08
$BaCe_{0.7}Ta_{0.1}Gd_{0.2}O_{3-\delta}$	1·00±0·034	0·75±0·025	0·21±0·006	0	0	0·08±0·003	4·384±0·064	84·292±3·710	85±1·05

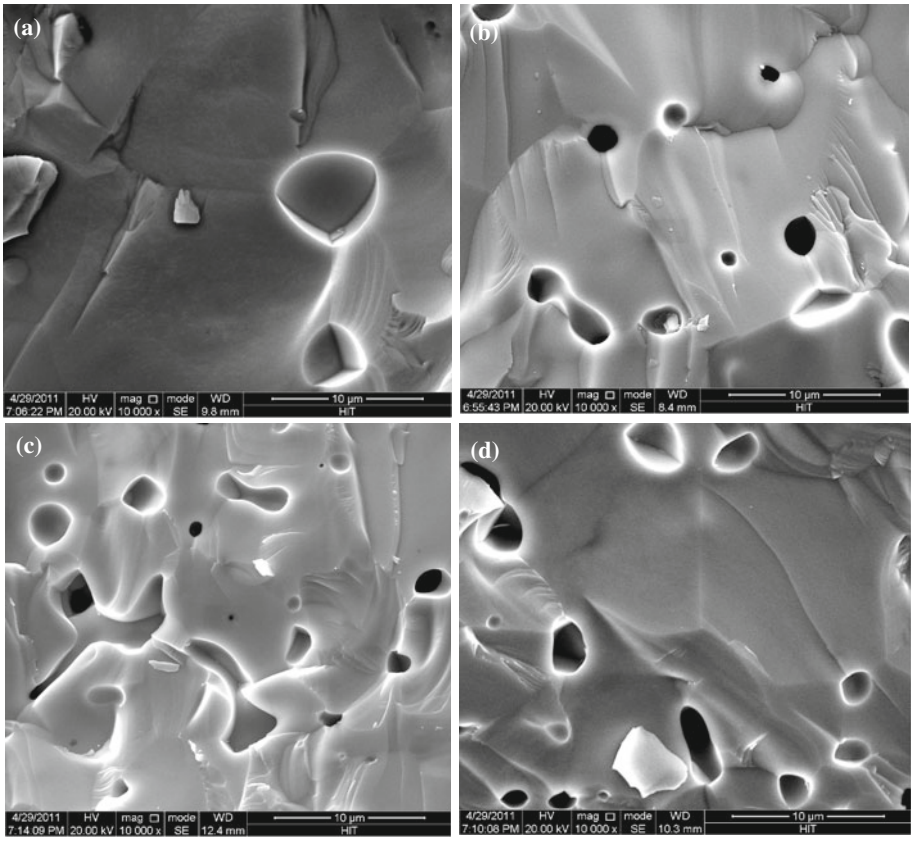

Figure 2. SEM micrographs of fractured surfaces of $BaCe_{0.8-x}A_xGd_{0.2}O_{3-\delta}$ ceramics sintered at 1973 K for 10 h: (**a**) $BaCe_{0.8}Gd_{0.2}O_{3-\delta}$, (**b**) $BaCe_{0.7}In_{0.1}Gd_{0.2}O_{3-\delta}$, (**c**) $BaCe_{0.7}Zr_{0.1}Gd_{0.2}O_{3-\delta}$ and (**d**) $BaCe_{0.7}Ta_{0.1}Gd_{0.2}O_{3-\delta}$.

XRD data are listed in table 1 with standard deviations. Clearly, molar ratio of metallic elements measured by EDS is in good agreement with the nominal stoichiometry within the experimental error. The unit cell volume decreases in the order of $BaCe_{0.8}Gd_{0.2}O_{3-\delta} > BaCe_{0.7}In_{0.1}Gd_{0.2}O_{3-\delta} > BaCe_{0.7}Zr_{0.1}Gd_{0.2}O_{3-\delta} > BaCe_{0.7}Ta_{0.1}Gd_{0.2}O_{3-\delta}$ in accordance with ionic radii of cations, which decreases in the order of $Gd^{3+} > In^{3+} > Zr^{4+} > Ta^{5+}$ in six coordination.

SEM micrographs of fractured surfaces of $BaCe_{0.8-x}A_xGd_{0.2}O_{3-\delta}$ ceramics sintered at 1973 K for 10 h are shown in figure 2. It can be seen that $BaCe_{0.8}Gd_{0.2}O_{3-\delta}$ and $BaCe_{0.7}In_{0.1}Gd_{0.2}O_{3-\delta}$ ceramics are relatively dense; however, $BaCe_{0.7}Zr_{0.1}Gd_{0.2}O_{3-\delta}$ and $BaCe_{0.7}Ta_{0.1}Gd_{0.2}O_{3-\delta}$ ceramics contain some small pores. Obviously, the co-doping of indium and gadolinium cations are favourable to the sintering densification, however, the situation is reversed when zirconium and Ta cations are doped. A dopant oxide with a low melting point and dopant ionic radius close to Ce cations are favourable to sintering. In the present work, melting point of In_2O_3 is lower than that of ZrO_2, which makes

$BaCe_{0.7}In_{0.1}Gd_{0.2}O_{3-\delta}$ ceramic much easier to be densified than $BaCe_{0.7}Zr_{0.1}Gd_{0.2}O_{3-\delta}$ ceramic. However, the melting point of Ta_2O_5 is very low and became volatile during sintering. Volatilization of Ta_2O_5 produces some pores in the sintered samples, which may block the conduction. In this study, relative densities of $BaCe_{0.8-x}A_xGd_{0.2}O_{3-\delta}$ samples sintered at 1973 K for 10 h are above 92%, except for Ta-doped sample of $BaCe_{0.7}Ta_{0.1}Gd_{0.2}O_{3-\delta}$, which has a relative density of 85% as shown in table 1.

3.2 *Electrical conductivity of $BaCe_{0.8-x}A_xGd_{0.2}O_{3-\delta}$ ceramics*

A.C. impedance spectra of $BaCe_{0.7}In_{0.1}Gd_{0.2}O_{3-\delta}$ ceramic measured in a temperature range of 573–1073 K in both air and dry hydrogen atmospheres are shown in figure 3. As a.c. impedance spectra of $BaCe_{0.8}Gd_{0.2}O_{3-\delta}$, $BaCe_{0.7}Zr_{0.1}Gd_{0.2}O_{3-\delta}$ and $BaCe_{0.7}Ta_{0.1}Gd_{0.2}O_{3-\delta}$ ceramics are quite similar to that of $BaCe_{0.7}In_{0.1}Gd_{0.2}O_{3-\delta}$ ceramic, a.c. impedance spectra of $BaCe_{0.7}In_{0.1}Gd_{0.2}O_{3-\delta}$ ceramic were chosen to demonstrate the evolution of typical impedance spectrum with temperature. Fitting of the impedance spectrum was carried out using Zview 2 software with appropriate equivalent circuit to distinguish bulk and the grain-boundary resistances. Total resistance of the electrolyte can be expressed as:

$$R_t = R_b + R_{gb}, \tag{5}$$

where R_t is the total resistance, R_b the bulk resistance and R_{gb} the grain-boundary resistance.

The impedance spectrum consists of a high frequency semicircular arc and a low frequency line (or arc), which are attributed to the response of grain boundaries and electrodes, respectively. Total resistance of electrolyte can be obtained from the spectra and conductivity is calculated using the relation:

$$\sigma = \frac{l}{R_t S}, \tag{6}$$

where l is the sample thickness, S the electrode area on the sample surface and R_t the total resistance.

The electrical conductivity gradually increases with increasing temperature from 573 to 1073 K. $BaCe_{0.7}In_{0.1}Gd_{0.2}O_{3-\delta}$ ceramic has the highest conductivity of $4{\cdot}6 \times 10^{-2}$ S·cm^{-1} at 1073 K in air. It is worth mentioning that the conductivity of $BaCe_{0.7}In_{0.1}Gd_{0.2}O_{3-\delta}$ is $1{\cdot}1 \times 10^{-2}$ S·cm^{-1} at 823 K in dry hydrogen atmosphere, which is higher than that (1×10^{-2} S·cm^{-1}) obtained in air. However, at

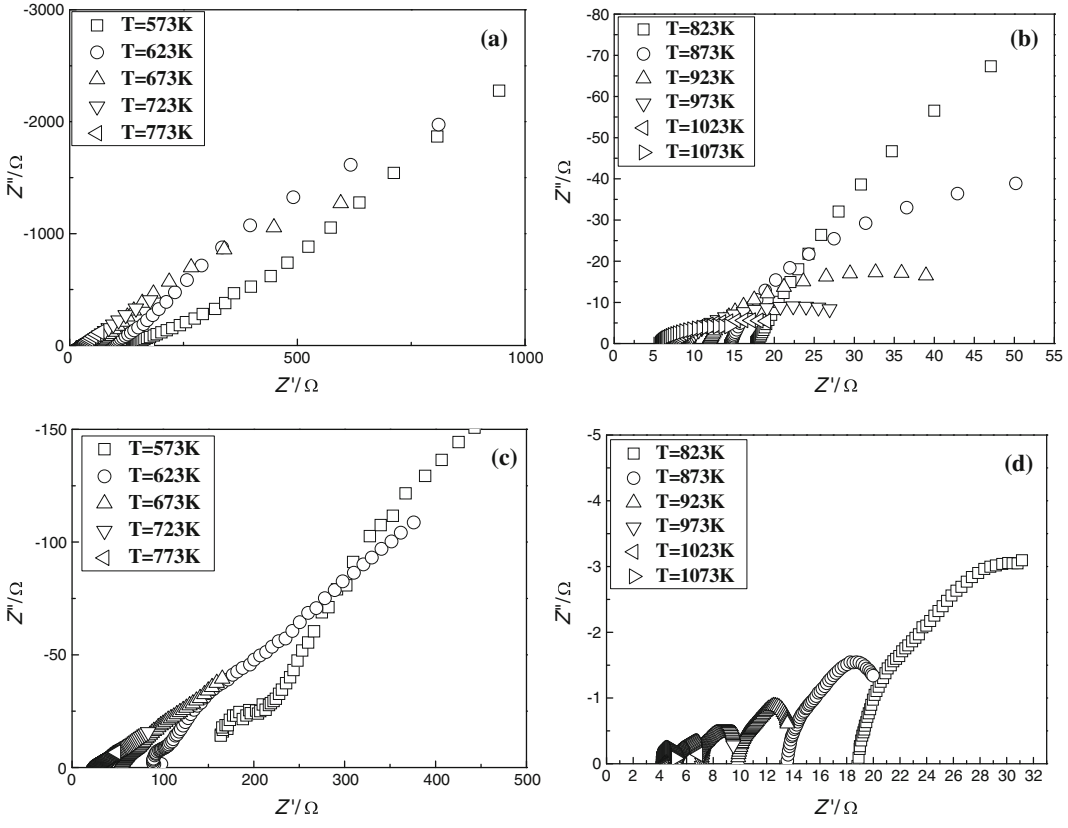

Figure 3. A.C. impedance spectra of $BaCe_{0.7}In_{0.1}Gd_{0.2}O_{3-\delta}$ ceramic measured in temperature range of 573–1073 K in both air and dry hydrogen atmospheres: (**a**) in dry hydrogen at temperatures of 573–773 K, (**b**) in dry hydrogen at temperatures of 823–1073 K, (**c**) in air at temperatures of 573–773 K and (**d**) in air at temperatures of 823–1073 K.

1073 K, the conductivity of $BaCe_{0.7}In_{0.1}Gd_{0.2}O_{3-\delta}$ is $3{\cdot}2 \times 10^{-2}$ S·cm^{-1} in dry hydrogen atmosphere, which is lower than that ($4{\cdot}6 \times 10^{-2}$ S·cm^{-1}) obtained in air. It suggests that proton conductivity is predominant at relatively low temperature such as 823 K, however, oxide–ion conductivity becomes main contributor at relatively high temperature such as 1073 K. Guan *et al* (1997) characterized the transport properties of a mixed $BaCe_{0.95}Y_{0.05}O_{3-\alpha}$ by measuring the open cell voltage (OCV) of $BaCe_{0.95}Y_{0.05}O_{3-\alpha}$ in different atmospheres. The protons dominate ionic conduction in the temperature range of 773–873 K in an oxygen/water vapour atmosphere, while oxygen ions could dominate at higher temperatures of 973–1073 K. They also found that proton conduction dominates over the entire temperature range of 773–1073 K in a hydrogen/water vapour atmosphere (Guan *et al* 1997). Thus, in the present work, the proton conduction is predominant at low temperature such as 823 K. However, at high temperature such as 1073 K, the oxide–ions in air are more suitable than proton in hydrogen to take the conduction duty. Arrhenius plots of total conductivity of $BaCe_{0.8-x}A_xGd_{0.2}O_{3-\delta}$ ceramics at intermediate temperatures of 573–1073 K in both air and dry hydrogen atmospheres are shown in figure 4. The conductivities of $BaCe_{0.8}Gd_{0.2}O_{3-\delta}$ and $BaCe_{0.7}In_{0.1}Gd_{0.2}O_{3-\delta}$ ceramics are higher than those of other ceramics in both air and dry hydrogen atmospheres. From table 1, $BaCe_{0.8}Gd_{0.2}O_{3-\delta}$, $BaCe_{0.7}In_{0.1}Gd_{0.2}O_{3-\delta}$ and $BaCe_{0.7}Zr_{0.1}Gd_{0.2}O_{3-\delta}$ ceramics have a high relative density than $BaCe_{0.7}Ta_{0.1}Gd_{0.2}O_{3-\delta}$ ceramic. $BaCe_{0.7}Ta_{0.1}Gd_{0.2}O_{3-\delta}$ ceramic with the lowest relative density has a lowest electrical conductivity among all the ceramics. This indicates that a dense perovskite structure seems to be beneficial to the conduction. Oxygen vacancies, which are responsible for oxide–ion and proton conduction, are introduced into the perovskite structure when Ce^{4+} cations are partially substituted by the trivalent cations of Gd^{3+} and In^{3+} cations. Therefore, there are more oxygen vacancies in $BaCe_{0.8}Gd_{0.2}O_{3-\delta}$ and $BaCe_{0.7}In_{0.1}Gd_{0.2}O_{3-\delta}$ ceramics, which have a relatively higher conductivity and have the potential to be used as a solid electrolyte in an intermediate-temperature SOFC. The activation energy (E_a) and pre-exponential term (A) are obtained by linear fitting of Arrhenius plots and the results are shown in table 2. The activation energy in dry hydrogen is 0·3–0·4 eV, which is smaller than that (0·4–0·5 eV) in air due to the nature of protonic conduction.

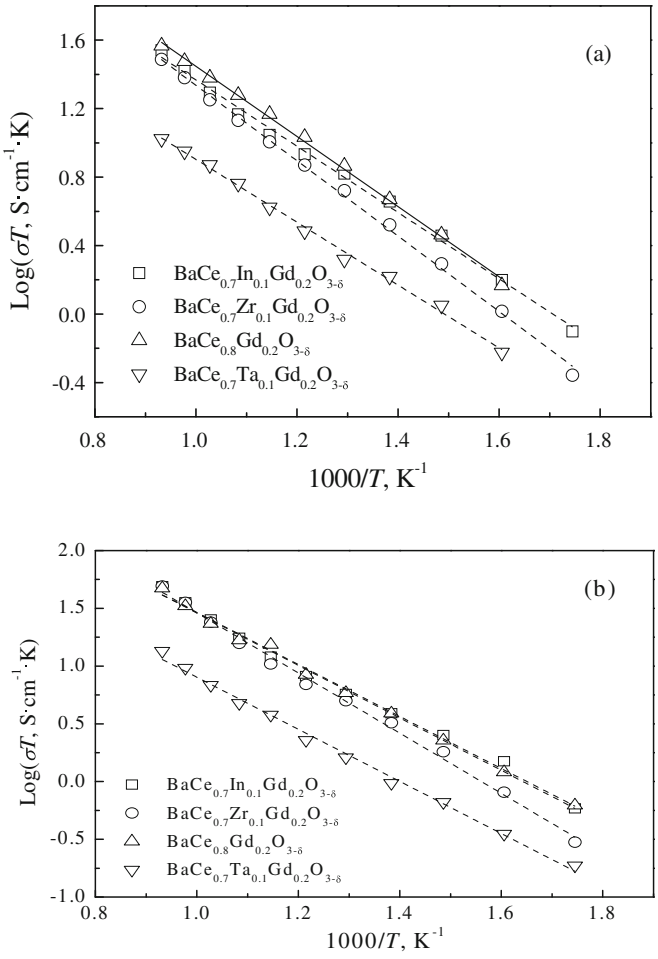

Figure 4. Arrhenius plots of total conductivity of $BaCe_{0.8-x}A_xGd_{0.2}O_{3-\delta}$ ceramics at intermediate temperatures of 573–1073 K: (**a**) in dry hydrogen atmosphere and (**b**) in air atmosphere.

3.3 *Chemical stability of $BaCe_{0.8-x}A_xGd_{0.2}O_{3-\delta}$ ceramics against boiling water*

As mentioned above, $BaCe_{0.7}In_{0.1}Gd_{0.2}O_{3-\delta}$ and $BaCe_{0.8}Gd_{0.2}O_{3-\delta}$ ceramics exhibit high conductivity at low temperatures such as 823 K. Therefore, they have the potential to be used as a solid electrolyte in an intermediate temperature SOFC. However, as the water vapour is produced at the cathode side, in H_2O-containing atmosphere, the conventional

Table 2. Activation energy (E_a) and pre-exponential term (A) for conductivity of $BaCe_{0.8-x}A_xGd_{0.2}O_{3-\delta}$ ceramics sintered at 1973 K for 10 h.

Samples	E_a (H_2)	E_a (air)	A (H_2)	A (air)
$BaCe_{0.8}Gd_{0.2}O_{3-\delta}$	0·392	0·435	3138·846	5389·147
$BaCe_{0.7}In_{0.1}Gd_{0.2}O_{3-\delta}$	0·371	0·431	5179·168	11678·85
$BaCe_{0.7}Zr_{0.1}Gd_{0.2}O_{3-\delta}$	0·422	0·499	2014·884	3448·657
$BaCe_{0.7}Ta_{0.1}Gd_{0.2}O_{3-\delta}$	0·351	0·432	548·3653	1441·518

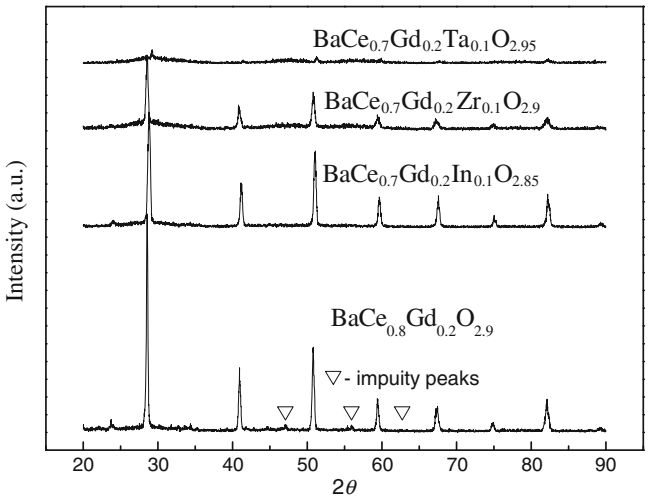

Figure 5. XRD patterns of $BaCe_{0.8-x}A_xGd_{0.2}O_{3-\delta}$ ceramics exposed to boiling water for 2 h.

solid electrolyte of doped $BaCeO_3$ does not always possess sufficient chemical stability, and looses its proton conductivity (Tanner *et al* 1992). Thermodynamically, it easily decomposes into CeO_2 and $Ba(OH)_2$, according to the following reaction:

$$BaCeO_3 + H_2O \leftrightarrow Ba(OH)_2 + CeO_2. \quad (7)$$

Figure 5 shows XRD patterns of $BaCe_{0.8-x}A_xGd_{0.2}O_{3-\delta}$ ceramics exposed to boiling water for 2 h. Clearly, $BaCe_{0.7}In_{0.1}Gd_{0.2}O_{3-\delta}$ and $BaCe_{0.7}Zr_{0.1}Gd_{0.2}O_{3-\delta}$ ceramics exhibit good chemical stability. No obvious changes in phase constituents for $BaCe_{0.7}In_{0.1}Gd_{0.2}O_{3-\delta}$ and $BaCe_{0.7}Zr_{0.1}Gd_{0.2}O_{3-\delta}$ ceramics are found before and after the pellets are exposed to the boiling water. Some small impurity peaks appear in XRD pattern of $BaCe_{0.8}Gd_{0.2}O_{3-\delta}$ ceramic, however, the diffraction peaks of cubic perovskite structure almost disappear in XRD pattern of $BaCe_{0.7}Ta_{0.1}Gd_{0.2}O_{3-\delta}$ ceramic. It is mainly due to high porosity of as-sintered $BaCe_{0.7}Ta_{0.1}Gd_{0.2}O_{3-\delta}$ pellets by conventional solid-state reaction method. Indium is a suitable doping element to promote the sintering densification and to enhance both the electrical conductivity and chemical stability of Gd-doped $BaCeO_3$ at operating temperatures.

4. Conclusions

$BaCe_{0.8-x}A_xGd_{0.2}O_{3-\delta}$ (A = In, Zr, Ta; $x = 0, 0{\cdot}1$) ceramics are successfully synthesized by solid-state reaction method. $BaCe_{0.8}Gd_{0.2}O_{3-\delta}$, $BaCe_{0.7}In_{0.1}Gd_{0.2}O_{3-\delta}$ and $BaCe_{0.7}Zr_{0.1}Gd_{0.2}O_{3-\delta}$ ceramics exhibit a single cubic perovskite structure. The relative density of $BaCe_{0.8-x}A_xGd_{0.2}O_{3-\delta}$ ceramics is above 92%, except for $BaCe_{0.7}Ta_{0.1}Gd_{0.2}O_{3-\delta}$ ceramic. The electrical conductivity gradually increases with increasing temperature from 573 to 1073 K. $BaCe_{0.7}In_{0.1}Gd_{0.2}O_{3-\delta}$ ceramic has the highest conductivity of $4{\cdot}6 \times 10^{-2}$ S·cm^{-1} in air at 1073 K. For $BaCe_{0.7}In_{0.1}Gd_{0.2}O_{3-\delta}$, proton conductivity is predominant at 823 K, while oxide–ion conductivity becomes the main contribution at 1073 K. $BaCe_{0.7}In_{0.1}Gd_{0.2}O_{3-\delta}$ and $BaCe_{0.7}Zr_{0.1}Gd_{0.2}O_{3-\delta}$ ceramics exhibit excellent chemical stability against boiling water. Indium is a suitable doping element to promote the sintering densification and to enhance both the electrical conductivity and chemical stability of Gd-doped $BaCeO_3$ at operating temperatures.

Acknowledgements

This work was financially supported by the National Natural Science Foundation of China (NSFC, Grant Nos. 50972030, 51021002 and 51272054) and the Fundamental Research Funds for the Central Universities (Grant No. HIT.BRET1.2010006).

References

Bonanos N, Knight K S and Ellis B 1995 *Solid State Ionics* **79** 161
Chen C and Ma G L 2009 *J. Alloys Compd.* **485** 69
Chen F, Toft Sørensen O, Meng G and Peng D 1998 *J. Eur. Ceram. Soc.* **18** 1389
Chiodelli G *et al* 2009 *J. Alloys Compd.* **470** 477
Choudhury P, Srinivasan S S, Bhethanabotla V R, Goswami Y, McGrath K and Stefanakos E K 2009 *Int. J. Hydrogen Energy* **34** 6325
Demin A K, Tsiakaras P E, Sobyanin V A and Hramova S Y 2002 *Solid State Ionics* **152** 555
Fabbri E, Epifanio D A, Bartolomeo E D, Licoccia S and Traversa E 2008 *Solid State Ionics* **179** 558
Guan J, Dorris S E, Balachandran U and Liu M 1997 *Solid State Ionics* **100** 45
Guan J, Dorris S E, Balachandran U and Liu M 1998 *J. Electrochem. Soc.* **145** 1780
Haile S M 2003 *Acta Mater.* **51** 5981
Ishihara T, Yan J W, Shinagawa M and Matsumoto H 2006 *Electrochim. Acta* **52** 645
Iwahara H, Esaka T, Uchida H and Maeda N 1981 *Solid State Ionics* **3/4** 359
Jacob K T, Jain S, Saji V S and Srikanth P V K 2010 *Bull. Mater. Sci.* **33** 407
Khandelwal M, Venkatasubramanian A, Prasanna T R S and Gopalan P 2011 *J. Eur. Ceram. Soc.* **31** 559
Kreuer K D 2003 *Annu. Rev. Mater. Res.* **33** 333
Künstler K, Lang H J, Maiwald A and Tomandle G 1998 *Solid State Ionics* **107** 221
Li T S, Wang W G, Miao H, Chen T and Xu C 2010 *J. Alloys Compd.* **495** 138
Liou Y C and Yang S L 2008 *J. Power Sources* **179** 553
Liu Z-G, Gao S, Ouyang J-H and Xia X-L 2010 *J. Alloys Compd.* **506** 868
Mclntosh S and Gorte R J 2004 *Chem. Rev.* **104** 4845
Norby T and Larring Y 2000 *Solid State Ionics* **136** 139
Pelletier L, McFarlan A and Maffei N 2005 *J. Power Sources* **145** 262
Peng R, Wu Y, Yang L and Mao Z 2006 *Solid State Ionics* **177** 389

Tanner C W, Jue J F and Virkar A 1992 *J. Electrochem. Soc.* **2** 126
Uehara T, Koto K, Kanamaru F and Horiuchi H 1987 *Solid State Ionics* **23** 137
Virkar A N and Maiti H S 1985 *J. Power Sources* **14** 295
Wang J, Li L, Campbell B, Lv Z, Ji Y, Xue Y and Su W 2004 *Mater. Chem. Phys.* **86** 150
Wu Z and Liu M 1997 *J. Electrochem. Soc.* **144** 2170
Zhang C J and Zhao H L 2010 *Solid State Ionics* **181** 1478
Zhang H, Liu H, Cong Y and Yang W 2008 *J. Power Sources* **185** 129
Zuo C, Zha S, Liu M, Hatano M and Uchiyama M 2006 *Adv. Mater.* **18** 3318